Evolution of Order in Thin Block Copolymer Films

A. M. Mayes

Massachusetts Institute of Technology, Cambridge, Massachusetts 02139

T. P. Russell*

IBM Research Division, Almaden Research Center, 650 Harry Road, San Jose, California 95120-6099

P. Bassereau

Institut Curie, Paris, France

S. M. Baker and G. S. Smith

Los Alamos National Laboratory, Los Alamos, New Mexico 87545

Received September 7, 1993; Revised Manuscript Received November 8, 1993®

ABSTRACT: The organization of thin films of symmetric poly(styrene-*b*-methyl methacrylate) diblock copolymers on silicon is investigated by neutron and X-ray reflectivity. The surface and internal structure as a function of annealing time is compared for two sets of films 680 and 800 Å in thickness. For the thicker films the equilibrium morphology shows no surface features since the film thickness is $2.5L$ where L is the period of the lamellar microdomain morphology. The thinner films, $2.1L$ in thickness, exhibit hole formation over 40% of the surface. In both cases the multilayer organization proceeds from the substrate upward by chain transport through channels which perforate the developing layers. For short annealing times a sharp increase in surface roughness is seen, which may be linked with the wetting of PMMA-rich surface regions by polystyrene. At longer times these height fluctuations decay or grow into holes, depending on the initial film thickness.

1. Introduction

Nearly 20 years of fundamental research on block copolymers have shed much light on the nature of these fascinating and technologically important materials. The localized segregation of chemically dissimilar blocks into ordered microdomains is now generally well understood from a thermodynamic standpoint.[1] Yet recent discoveries of interconnected-lamellar morphologies[2,3] and entropy-driven disorder–order transitions[4] suggest that our current picture for the phase diagram of copolymer melts is still incomplete. Moreover, very little is known about the mechanisms for copolymer diffusion[5–7] and the dynamics of the ordering process.[8,9]

In a thin-film geometry a strong oreintation aspect is additionally introduced into the dynamics and thermodynamics of copolymer organization. Surface energy differences between the block components or the chemical affinity of one block for the substrate forces the orientation of lamellae or cylinders parallel to the film surface.[10–13] For diblock copolymers with nearly symmetric compositions, this preferred orientation causes a quantization of the film height to $(n + {}^1/_2)L$ or nL, where L is the bulk value of the copolymer lamellar period and n is an integer. For films with thicknesses which do not initially satisfy this constraint, islands or holes with a step height of L are formed on the surface.

The phenomenon of island and hole formation or poly(styrene-*b*-methacrylate) film surfaces has been studied previously by Coulson and co-workers using optical and atomic force microscopy.[14,15] Their work suggests that the appearance of such surface features is preceded by a large increase in surface roughess in the early stages of annealing which progressively evolves into the island or hole topography. With further annealing the surface morphology coarsens, with the number of islands decreasing and the average size increasing. However, the mechanism by which the ordered multilayer structure of the film forms, and couples, to the mechanism of island or hole formation has not been addressed.

Here neutron and X-ray reflectivity studies are combined with optical microscopy to study the evolution of order and orientation in thin copolymer films and to elucidate the mechanism which controls the generation of the surface topography. X-ray reflectivity and optical microscopy provide information on the surface topography since the contrast between the PS and PMMA layers within the film is small in comparison to the contrast at the copolymer/air interface. By labeling the styrene block with deuterium, the organization of the lamellar microdomains within the film can be studied concurrently with neutron reflectivity.

For this investigation thin films of a symmetric diblock copolymer, comprised of a perdeuterated polystyrene block and a normal poly(methyl methacrylate) block, denoted P(d-S-*b*-MMA), with a total molecular weight of 8×10^4, were deposited on silicon substrates. Here, PMMA segregates to the substrate while PS, the lower surface energy component, resides at the free surface.[11] Consequently, the equilibrium film thickness is given by $(n + {}^1/_2)L$, with $L = 320$ Å. To probe the mechanism of hole formation, two different film thicknesses were considered. Films $2.5L$ (800 Å) thick showed no surface structure while films $2.1L$ (680 Å) thick had a 40% coverage of holes on the film surface.

For short annealing times the reorganization of material is found to proceed similarly in the two cases studied. The planar orientation of the lamellar doamins is initiated by the strong interactions between the PMMA block and the oxide layer on the substrate. The PS half-layer at the free surface develops more slowly, and this process is always coupled with an amplified surface roughness. As annealing

® Abstract published in *Advance ACS Abstracts*, January 1, 1994.

0024-9297/94/2227-0749$04.50/0

proceeds, the surface roughness decays rapidly for the thicker film system, but develops as holes in the thinner system. Both processes are shown to be highly localized to the surface, with few accompanied changes in the interior film structure.

2. Experimental Section

A P(d-S-*b*-MMA) diblock copolymer having 52 vol % PS with $M_w = 8 \times 10^4$ and $M_w/M_n = 1.05$ was purchased from Polymer Laboratories. Homopolystyrene impurity, generated in the synthesis, was eliminated from the copolymer by Soxhlet extraction with cyclohexane. Matched sets of copolymer films, with thicknesses of 680 and 800 Å, were prepared by spin-coating P(d-S-*b*-MMA) solutions in toluene onto polished, 5-cm Si substrates purchased from Semiconductor Processing Co. Prior to use the substrates were placed in a Chromerge bath overnight and rinsed thoroughly with deionized water. The substrates were then immersed in a bath of sulfuric acid and Nochromix for 5 min, rinsed with deionized water, and placed in a 2-propanol vapor degreasing chamber for several minutes. Finally, the substrates were dried under a blanket of nitrogen at 110 °C. This procedure removes organic impurities from the surface and leaves an oxide layer of ~15 Å on the underlying Si.

The copolymer films were cast from 2% solution in toluene using syringes equipped with 1-μm Millipore filters to remove dust particles. The spinning speed was adjusted to obtain samples 2.5*L* and 2.1*L* in thickness. For a given set of films the standard deviation in thickness was ±10 Å as determined by optical ellipsometry. Films were annealed under vacuum at 170 ± 3 °C for times ranging from 0.1 h to 24 h. Once removed from the oven, samples were quenched to room temperatures by placing the substrates in contact with a thick Cu plate.

Subsequent to annealing, optical microscopy observations revealed no features on the surface of the 800-Å films. For the 680-Å films, macroscopic roughness was detected after annealing for 30 min. For films annealed 1 h or more, two distinct interference colors were observed, indicating the formation of holes at the surface. Coarsening of these hole structures was seen with increased annealing time, as described in other studies.[14,15]

Neutron reflectivity measurements were performed at the Manuel Lujan, Jr. Neutron Scattering Center at Los Alamos National Laboratory. The SPEAR reflectometer is a horizontal time-of-flight instrument equipped with a position-sensitive detector to allow simultaneous collection of specular and off-specular reflection data. In these experiments data were collected over a $k_{z,0}$ range from 0.004 to 0.06 Å^{-1}, where $k_{z,0}$ is the normal component of the incident neutron momentum in vacuum and is given by $2\pi \sin\theta/\lambda$ where λ is the wavelength and θ is the grazing angle of incidence. A detailed description of the instrument geometry and the data reduction procedure are published elsewhere.[16] Briefly, the resolution of the reflectometer, $\Delta k_{z,0}/k_{z,0}$, is 0.03. With a time-of-flight reflectometer equipped with a one-dimensional detector, both the specular reflectivity and the off-specular scattering are obtained simultaneously. This allows for a straightforward subtraction of the background. Data were collected on each of the samples over approximately 3 h at a beam current of 70 μA.

X-ray reflectivity measurements were performed using an 18-kW Rigaku rotating anode generator equipped with a copper target. A channel-cut Si monochromator delivered Cu Kα radiation onto the sample surface of wavelength 1.542 Å. To measure the specular reflectivity the sample is rotated θ and the detector 2θ with respect to the X-ray source. The incident and reflected beam intensities were measured with a scintillation detector using pulse-height analysis to remove electronic noise. Measurements were made up to $k_{z,0} = 0.14$ Å^{-1} to achieve a high sensitivity to surface roughness. The background subtracted from the specular was determined by measuring the reflectivity with the detector at +0.25° and −0.25° from the specular condition and averaging the two measurements. Due to the finite size of the specimen, the sample does not intercept the full beam at small incidence angles. This "footprint" can be taken into account by a simple geometric correction. However, this correction was not necessary for the purposes of the measurements described here. Consequently, it was not used. Fits to the reflectivity data were performed with a linear-least-squares iterative-fitting routine described in earlier publications.[17,18] Model composition profiles assumed alternating PS- and PMMA-rich layers with intervening composition gradients of hyperbolic tangent form. To fit the neutron data the b/V, thickness, and interfacial width were varied independently for all layers of the model. Once a coarse fit to the neutron data was obtained, the X-ray data was analyzed using the parameters derived from the neutron reflectivity experiments as an initial guess for the model electron-density profile. The fit to the neutron data was then refined using the X-ray results and the process repeated to obtain a concentration profile normal to the film surface that was consistent with both the X-ray and neutron reflectivity results.

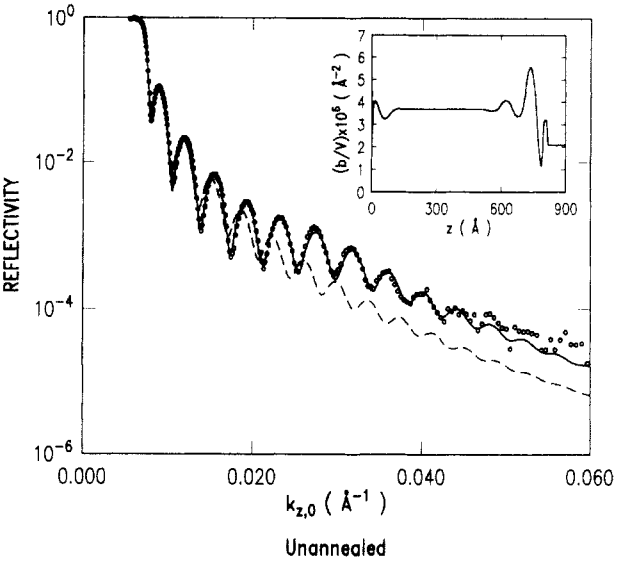

Figure 1. Neutron reflectivity profile for 800-Å film in the as-cast state. Dashed line through the data indicates best fit for a uniform film. Solid line corresponds to inset b/V profile. The air/polymer interface corresponds to 0 in the scattering length density profile.

3. Discussion of Results

Figure 1 shows neutron reflectivity data for an 800-Å film of P(d-S-*b*-MMA) as cast (open circles). The oscillations evident in the data result from interferences between neutrons reflected at the substrate and air interfaces and are thus characteristic of the film thickness.[18] However, analysis of these data reveals that the composition as a function of depth is not uniform. The dashed line in Figure 1 is the reflectivity profile calculated assuming that the scattering length density, b/V, is constant throughout the film and equal to the average b/V of the copolymer. As can be seen, the agreement between the calculated and measured profiles is poor above 0.01 Å^{-1}. The solid line in Figure 1 is the best fit to the experimental reflectivity profile which was calculated using the scattering length density profile shown in the inset. Here, highly damped oscillations originating from both the air and substrate interfaces had to be included in the b/V profile. Note that a 20-Å oxide layer of $b/V = 3 \times 10^{-6}$ Å^{-2} has also been incorporated into the model. A similar b/V profile is obtained for the unannealed 680-Å film. The first oscillation adjacent to the Si surface is particularly strong, reaching a b/V value very close to that of pure PMMA (1×10^{-6} Å^{-2}). These results suggest that during the time in which the P(d-S-*b*-MMA) solution and substrate were in contact prior to spinning, a copolymer monolayer was adsorbed onto the substrate, driven by the strong affinity of PMMA for the silicon oxide. This adsorbed monolayer has a pronounced influence on the organizational dynamics within the film during subsequent annealing.

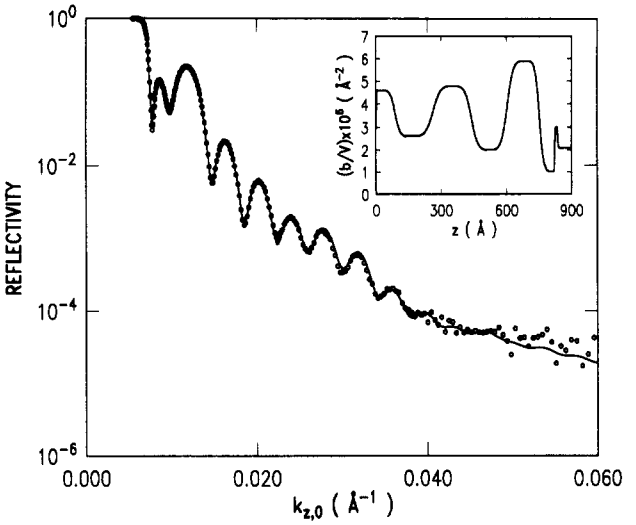

Figure 2. Neutron reflectivity profile for 800-Å film annealed 0.1 h. Solid line through data corresponds to inset b/V profile.

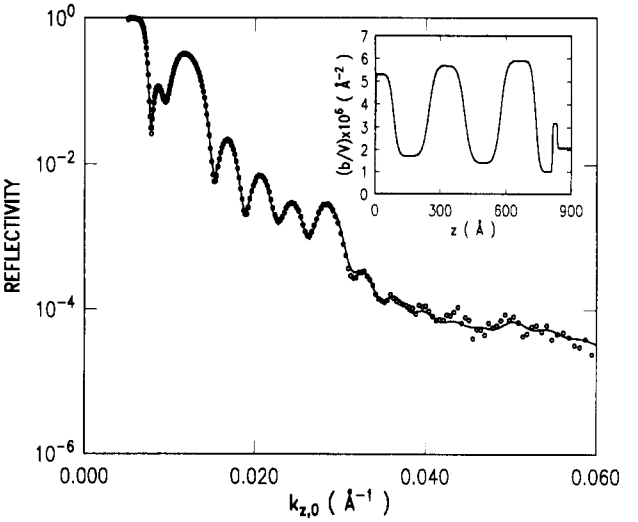

Figure 3. Neutron reflectivity profile and best-fit for 800-Å film annealed 0.25 h.

In the center of the as-cast films the scattering length density reflects a weighted average of the dPS ($b/V = 6.1 \times 10^{-6}$ Å^{-2}) and PMMA blocks. This might suggest that the film interior is uniformly mixed. Indeed, for 3×10^4 mol wt, PS–PMMA diblocks[12,19] and for other copolymer films in a phase-mixed state,[20] similar scattering length density profiles have been obtained. However, cross-section transmission electron microscopy on as-cast PS–PMMA films of 9×10^4 mol wt reveals a microphase-separated, aperiodic network morphology.[21] The characteristic length scale of the segregation normal to the film surface is $\sim 1/3$ the annealed lamellar period, in good agreement with the period obtained for the damped oscillations in Figure 1. During spin casting, fast evaporation of solvent from the surface rapidly increases the polymer concentration. This forces the system to cross over the spinodal into the ordered phase[22] as swollen chains collapse normal to the film surface. The spinning process could also introduce some degree of anisotropy in the chain conformation. TEM studies show that the characteristic size of the microphase-separated domains in a direction parallel to the film surface is comparable to the final lamellar period.[21]

Once the temperature of the film is raised to 170 °C (~70° above the glass transition), a rapid local relaxation of the copolymer chains occurs, establishing a new characteristic period normal to the surface that is close to the final lamellar spacing. The neutron reflectivity profile obtained for an 800-Å P(d-S-*b*-MMA) film annealed for only 6 min is shown in Figure 2. A first-order Bragg reflection is clearly seen in the data at $k_{z,0} \simeq 0.012$ Å^{-1}, superimposed on the Kiessig fringes. The best fit to the experimental data, indicated by the solid line in the figure, was obtained using the scattering length density profile shown in the inset. A layering scheme of $2.5L$ is adopted very early on, with the most complete ordering seen near the substrate. Apparently, the adsorbed copolymer monolayer creates a strong orientational field acting upon nearby chains. The PMMA-rich half-layer at the substrate and the adjacent dPS-rich layer display nearly pure component b/V values. However, the next PMMA-rich layer has a significant dPS content. The interfacial regions between this layer and the adjoining dPS-rich layers are additionally very broad (~70 Å). These results might be interpreted as evidence of weakly-segregated domains with diffuse boundaries.[19,20] However, TEM images of a highly segregated network structure even prior to annealing argue against this.[21] Instead we expect that the high b/V of this PMMA domain and the unusually broad interfaces are an indication of the presence of well-defined PS channels which perforate the PMMA layer. The channels connect the adjacent PS lamellae, forming low resistance paths along which copolymers can diffuse to establish the equilibrium structure. Similarly, channels of PMMA penetrate through the incomplete PS layers. Independent TEM studies have verified the existence of such interconnected morphologies in annealed PS–PMMA films on gold.[21]

As the PS layer nearest the substrate reaches an equilibrium thickness, the PS channels through the PMMA domains are closed and the effective interfacial width decreases substantially. Figure 3 shows the neutron reflectivity profile for an 800-Å film annealed for 0.25 h. A third-order Bragg reflection is now apparent in the data, indicating a highly oriented lamellar structure has formed. The scattering length density profile shown in the inset yielded the best fit to the reflectivity data as shown by the solid line in the figure. Comparing this scattering length density profile to that in Figure 2, it is seen that the organization of the multilayered structure is dominated by the organization at the substrate.

For films annealed 0.5 h or longer at 170 °C, the measured neutron reflectivity profiles are nearly identical. This suggests that the equilibrium film morphology is basically established within the first hour of annealing. Figure 4 shows the reflectivity data and the scattering length density profile that yielded the best fit to the experimental data after annealing the film for 4 h. The scattering length density profile is indicative of a highly oriented lamellar film with roughly uniform interfacial widths of 55 ± 5 Å between PS and PMMA microdomains. PS and PMMA layer thicknesses, shown as a function of annealing time in Table 1, provide further indication that the film morphology has equilibrated. The largest changes are seen over the first hour, with variations at later times due, most likely, to slight differences in initial film thickness.

Off-specular neutron data show very little diffuse scattering for the series of 800-Å films. With increased annealing, a band of diffuse intensity develops along $k_z = 0.012$ Å^{-1}, which intersects the primary Bragg reflection. This suggests that a small degree of correlated modulation exists in the final multilayered structure.[23,24] However, a quantitative analysis of the diffuse scattering is beyond the scope of this article.

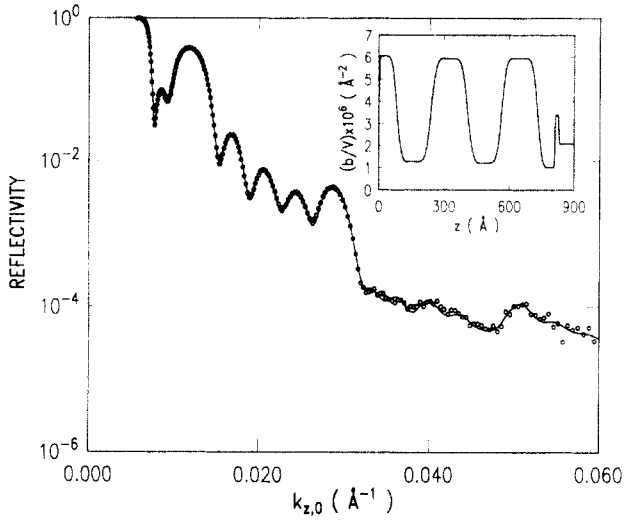

Figure 4. Neutron reflectivity profile and best-fit for 800-Å film annealed 4 h.

Table 1. Domain Thicknesses for 2.5L Films (Å)[a]

t (h)	PMMA	PS	PMMA	PS	PMMA	PS	total
0.1	70	148	165	176	175	89	823
0.1	70	148	165	176	175	89	823
0.5	70	162	161	168	161	85	807
1	77	163	153	165	155	84	797
4	80	166	157	167	158	83	811
8	76	167	157	169	159	86	814
24	76	165	150	162	150	81	784

[a] The error in the values of the individual layer thicknesses and in the total thickness is at most ±5 Å.

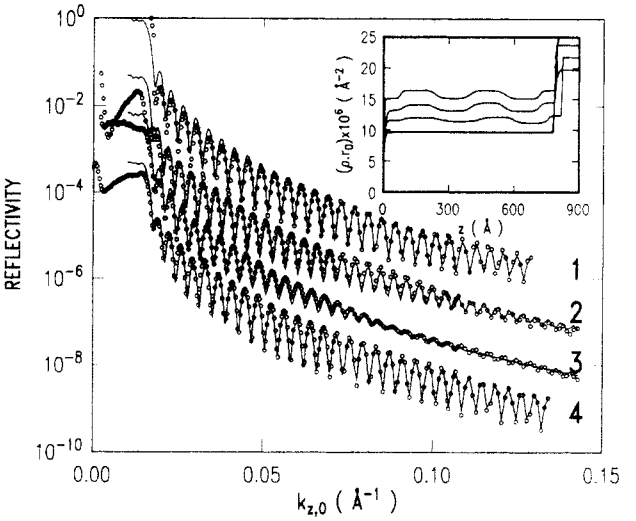

Figure 5. X-ray reflectivity profile and best-fits for 800-Å films annealed for various times: (1) 0 h, (2) 0.1 h, (3) 0.25 h, and (4) 4 h. Reflectivity curves and electron density profiles have been offset vertically for clarity.

To supplement the neutron reflectivity studies, X-ray reflectivity measurements were performed on the 800-Å films annealed for 0, 0.1, 0.25 and 4 h. Because the electron densities for PS and PMMA are quite similar, these measurements are mainly sensitive to the film/substrate and film/air interfaces. The X-ray profiles as a function of increased annealing time are shown in curves 1–4 of Figure 5, along with the corresponding electron density profiles which yielded the best fit to the data. Both the reflectivity profile and the scattering length density profiles have been offset vertically for clarity. The internal film structures used in the fits are consistent with results obtained from neutron measurements. However, as expected, fits to the X-ray data were insensitive to the internal structure of the film.

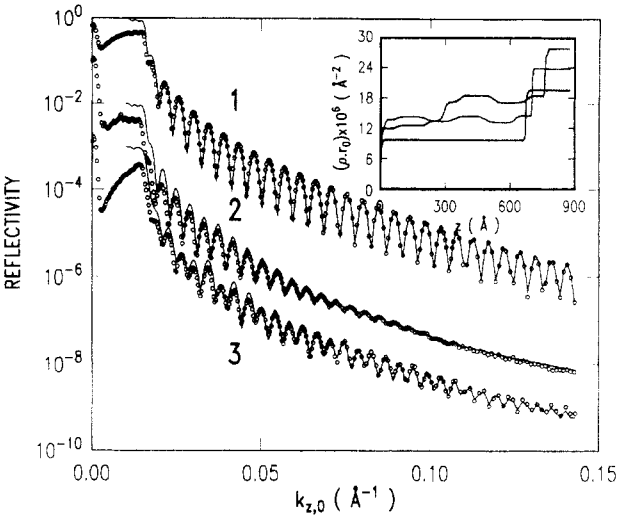

Figure 6. X-ray reflectivity profiles and best-fits for 680-Å films annealed for various times: (1) 0 h, (2) 0.25 h, (3) 4 h. Reflectivity curves and electron density profiles have been offset vertically for clarity.

A surprising observation from Figure 5 is that even if films ultimately exhibit no surface features (i.e., islands or holes), the organizational process is nevertheless characterized by extensive surface roughness. The highest roughness is seen after annealing the film for 0.25 h (curve 3). In the reflectivity profile, the thickness oscillations are markedly damped over a large range of $k_{z,0}$. The best fit to these data indicates a surface roughness $a_1 = (2\pi\sigma^2)^{1/2}$ (= 35 Å) where σ^2 is the mean square roughness assuming Gaussian statistics to define the deviation of the surface height away from the mean value. Although we do not have a definitive explanation for the origin of this unexpectedly high value, a reexamination of the neutron results for this system proves insightful. While general material transport processes within the film could certainly contribute to the roughness, the majority of the internal reorganization is apparently completed by this time, as suggested from Figure 3. However, a significant fraction of PMMA still remains at the film surface, around 15% as compared to 40% in the as-cast state. The slight difference in surface energy between the blocks could be driving a wetting process whereby PS blocks diffuse over the PMMA surface regions. This would require cooperative motion of the PMMA blocks, being chemically joined to polystyrene. Such a process would be characterized by fluctuations in film height on the order of R_G for a copolymer block. Alternatively, the enhanced roughness may result simply from an incomplete orientation of the lamellar microdomains parallel to the surface. If these domains are oriented at some angle with respect to the surface, there would be a tendency for the truncation of the lamellae at the surface to create a rough surface. In both cases, continued annealing causes further reorganization with the completion of the PS surface half-layer. This would be followed by a sharp decay in surface roughness, as observed in the X-ray data for the 4-h sample (curve 4). For this film strong Kiessig fringes are observed over the full range of data. The surface roughness for this sample determined from X-ray measurements was 12 Å, a value quite comparable to that of the as-cast films.

At early annealing times a similar organizational behavior is observed for the 2.1L thick sample. Shown in Figure 6 are the X-ray reflectivity profiles for the 680-Å

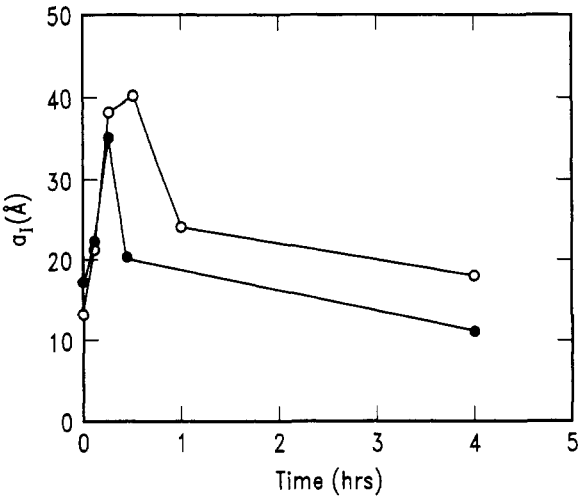

Figure 7. Surface roughness from fitted X-ray data for 800-Å (●) and 680-Å (○) films as a function of annealing time.

(2.1L) films as-cast and annealed for 0.25 and 4 h at 170 °C, curves 1–3, respectively. After 0.25 h the surface roughness increases to 38 Å, comparable to that of the thicker film annealed for a corresponding period. The Kiessig fringes are again heavily damped with increasing $k_{z,o}$. After 4-h annealing, the Kiessig fringes extend out to larger $k_{z,o}$, indicating a decrease in surface roughness averaged over the coherence length of the X-rays. Shown in the inset are the electron density profiles that yielded the best fit to the reflectivity results. The calculated profiles are shown as the solid lines in the figure. From these model electron density profiles an increase in the total film thickness is seen, and two distinct levels of electron density are apparent. The initial height fluctuations thus evolve into quantized film thicknesses of 1.5L and 2.5L for this system of films, as was observed by Coulon and co-workers.[14,15] The reduced level of electron density at the air surface is a direct ramification of holes forming on the surface and the electron density reflects the fractional coverage on the surface.

It is worthwhile to compare the development of roughness at the air surface as a function of time for the 2.1L and 2.5L thick specimens. Shown in Figure 7 is the surface roughness as a function of annealing time. In both cases a_I increases rapidly and, in fact, one cannot discern a difference between the two data sets. However, for the 2.5L thick specimen, a_I begins to decrease quite rapidly, much more so than for the 2.1L thick specimen. For the 2.1L thick sample, a_I continues to increase with time and is followed by a rapid decrease. The fact that the two are indistinguishable initially suggests that the origin of the surface roughness is the same. The rapid relaxation of the 2.5L thick sample roughness results from the easy accommodation of the copolymer chains into the multilayered structure. However, for the 2.1L sample, the incomplete layer at the air surface mandates the formation of holes which are, initially, not well formed. Consequently, the roughness decreases more slowly as the holes coarsen with time.

The neutron reflectivity data further illustrates the hole-formation process. Scattering length density profiles obtained from fitting the neutron reflectivity data for films annealed from 0 to 16 h are shown in Figure 8. Profiles for the as-cast, 0.1- and 0.25-h samples closely resemble those obtained for the thicker films shown in Figures 1–3. For longer times however, the scattering length densities of the surface dPS-rich half-layer decreases, while the total film thickness, derived from the Kiessig fringes, appears

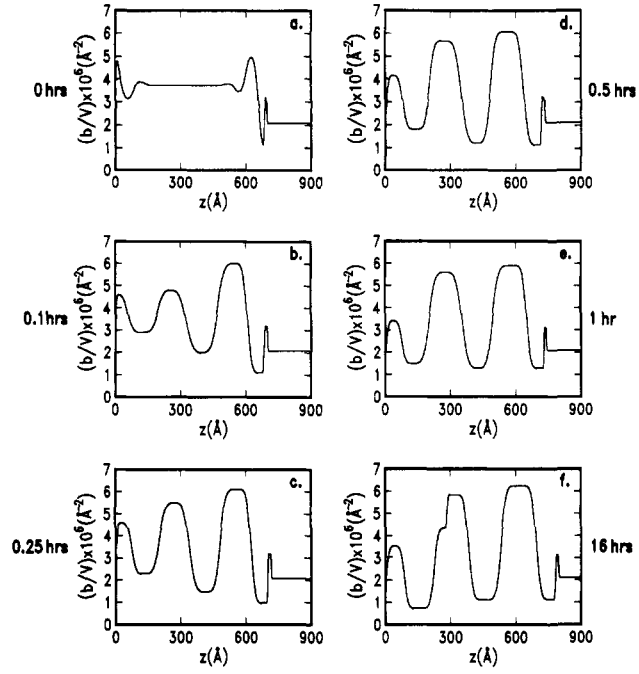

Figure 8. Best-fit scattering length density profiles for 680-Å films annealed for various times: (1) 0 h, (2) 0.1 h, (3) 0.25 h, (4) 0.5 h, (5) 1 h, and (6) 16 h. Reflectivity curves and electron density profiles have been offset vertically for clarity.

Table 2. Domain Thicknesses for 2.1L Films (Å)[a]

t (h)	PMMA	PS	PMMA	PS	PMMA	PS	total
0.1	76	136	145	129	139	58	683
0.25	76	141	142	136	129	77	701
0.5	80	151	135	145	123	80	714
1	80	155	141	149	127	76	728
16	87	161	150	158	137	87	780

[a] The error in the values of the individual layer thicknesses and in the total thickness is at most ±5 Å.

to increase (Table 2). These two trends are coupled. Since the total amount of deposited material must be conserved, the increase in the effective film thickness is possible only by the development of areas depleted of copolymers, namely holes. The lateral averaging of the scattering length density over the coherence length of the neutrons, i.e. microns, gives rise to an apparent decrease in the scattering length density of the uppermost layer. As these surface fluctuations develop into holes of an integral period in height, the effective scattering length density seen by the neutrons is reduced over a full period from the surface. This is clearly demonstrated in Figure 8 in the profile obtained for a film annealed for 16 h. Note that the apparent value of the scattering length density of the half-layer of dPS at the surface is $\sim 3.6 \times 10^{-6}$ Å^{-2}. This is ~60% of the scattering length density of a pure dPS layer (6.1×10^{-6} Å^{-2}) and is consistent with 40% of the surface being occupied by holes.

As the surface structure evolves, the PMMA and the PS layers closest to the substrate also increase slightly in thickness (Table 2), indicating that some degree of material transport occurs between the upper and lower regions of the film. However, the lower layers show little, if any, change in the scattering length density or interfacial width and appear as nearly pure block layers. By contrast, these parameters vary dramatically for the layers near the surface over the course of annealing. Thus, the hole formation process appears to involve primarily a reorganization and transport of material near the film/air interface.

Here we note that the quality of the fits for the 2.1L samples annealed beyond 0.5 h is noticeably poorer at

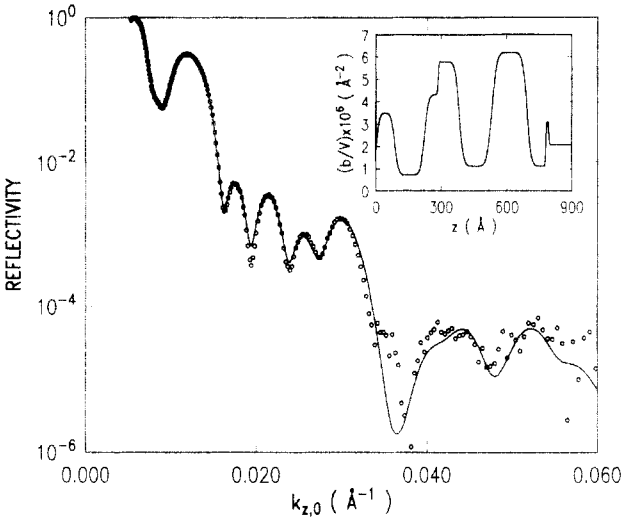

Figure 9. Neutron reflectivity profile for 680-Å film annealed 16 h. Solid line through data corresponds to inset b/V profile.

high angles. This is illustrated in Figure 9, which presents the fitted data for a 680-Å film annealed 16 h. For these films the diffuse scattering component becomes a substantial fraction of the total scattering intensity, particularly at high $k_{z,0}$. In fact it is problematic to determine the proper amount of background to subtract from the original data to obtain the true specular reflectivity. A rigorous analysis of the data would require fitting both the off-specular and specular contributions, as discussed by Sinha and co-workers[25-27] and addressed by Cai et al.[28] Here we have concentrated on the specular data to provide a general picture of the internal mechanism for step formation at the film surface. Analysis of the diffuse scattering is deferred to future articles.

4. Conclusions

In this study we found that copolymer organization in thin films appears to have several associated time scales. Immediately on heating, a very fast local rearrangement of chains occurs, relaxing the nonequilibrium microphase-separated morphology formed during the film deposition. The resulting three-dimensional segregated network structure provides a system of pathways for low-resistance diffusion of chains along the PS-PMMA interface. On the scale of minutes at 170 °C, an oriented multilayer front travels from the substrate upwards, fed by these channels which perforate the lamellae.[21] As the lamellar domains reach equilibrium thickness, the channels become unstable and dissolve into the lamellar structure. At the film/air interface, PS blocks gradually wet the PMMA at the surface, causing height fluctuations which ultimately decay or otherwise develop into steps, depending on the initial film thickness. The latter process proceeds on the time scale of hours, as evidenced by the continuous variation in domain sizes and the total film thickness with annealing time.

The formation of surface step structures is a phenomenon unique to finite dimensional copolymer systems. However, other aspects of the organizational process described here should be equally applicable to bulk-quenched copolymer systems. While there has been some progress in characterizing the growth of the lamellar phase from a metastable disordered phase,[8,9] the evolution of deeply-quenched bulk systems is likely to be more analogous to the process detailed here. Specifically, the propagation of multilayer fronts could proceed in a similar manner in bulk systems, with chain transport accomplished via channels between the developing lamellar domains and an intermediate segregated network structure. Bicontinuous networks and interconnected lamellar phases have now been observed in a number of copolymer systems, either as stable or metastable morphologies.[2,3,29-31]

The symmetric diblock used in this study has a χN value at 170 °C of 32, well above the mean-field critical point value of 10.5. In this region of the phase diagram little is known about diffusion mechanisms for copolymer chains. One would expect perfect multilayer morphologies to exhibit a high potential barrier to diffusion normal to the lamellae.[5,32] In recent reflectivity studies on thin-film bilayers of perdeuterated PS-PMMA copolymer and hydrogenated PS-PMMA copolymer, we found little or no interdiffusion normal to the lamellae once the ordering process was complete.[33] Diffusion in the parallel direction might also be expected to decrease relative to the disordered phase. For entangled copolymer melts, it has been suggested that diffusion along the interface would require retraction of the blocks toward the interface, a process analogous to star polymer reptation.[7,34] However, experiments on bulk systems which form lamellar phases have thus far shown no significant decrease in the diffusion coefficient upon crossing the order-disorder transition.[6,7] Is diffusion in the parallel direction more aptly described as linear chain reptation confined to the interphase? The broad distribution of junction points recently determined across the interphase regions of oriented PS-PMMA lend support for this description.[35]

Acknowledgment. LANSCE is supported by the U.S. Department of Energy under contract W-7405-ENG-36 with the University of California. This work was supported by the U.S. Department of Energy Office of Basic Energy Sciences under contract DE-FG03-88ER45375.

References and Notes

(1) See Vavasour, J. D.; Whitmore, M. D. *Macromolecules* **1992**, *25*, 5477, and refs therein.
(2) Almdahl, K.; Koppi, K. A.; Bates, F. S.; Mortensen, K. *Macromolecules* **1992**, *25*, 1743.
(3) Disco, M. M.; Liang, K. S.; Behal, S. K.; Roe, R. J.; Jeon, K. J. *Macromolecules* **1993**, *26*, 2983.
(4) Russell, T. P. Unpublished.
(5) Inoue, T.; Kishine, M.; Nemoto, N.; Kurata, M. *Macromolecules* **1989**, *22*, 494.
(6) Shull, K. R.; Kramer, E. J.; Bates, F. S.; Rosedale, J. H. *Macromolecules* **1991**, *24*, 1383.
(7) Ehlich, D.; Takenaka, M.; Hashimoto, T. *Macromolecules* **1993**, *26*, 492.
(8) Fredrickson, G. H.; Binder, K. *J. Chem. Phys.* **1989**, *91*, 7265.
(9) Paquette, G. C. *Phys. Rev. A* **1991**, *44*, 6577.
(10) Henkee, C. S.; Thomas, E. L.; Fetters, L. J. *J. Mater. Sci.* **1988**, *23*, 1685.
(11) Russell, T. P.; Coulon, G.; Deline, V. R.; Green, P. F. *Macromolecules* **1989**, *22*, 4600.
(12) Anastasiadis, S. H.; Russell, T. P.; Satija, S. K.; Majkrzak, C. F. *Phys. Rev. Lett.* **1989**, *62*, 1852.
(13) Anastasiadis, S. H.; Russell, T. P.; Satija, S. K.; Majkrzak, C. F. *J. Chem. Phys.* **1990**, *92*, 5677.
(14) Coulon, G.; Collin, B.; Ausserre, D.; Chatenay, D.; Russell, T. P. *J. Phys. Fr.* **1990**, *52*, 2801.
(15) Collin, B.; Chatenay, D.; Coulon, G.; Ausserre, D.; Gallot, Y. *Macromolecules* **1992**, *25*, 1621.
(16) Smith, G. S.; Hamilton, W. A. In *Condensed Matter Research at LANSCE*; Hyer, D. K., Ed.; (LALP 90-7) Los Alamos National Laboratory Report, 1990.
(17) Russell, T. P.; Menelle, A.; Anastasiadis, S. H.; Satija, S. K.; Majkrzak, C. F. *Macromolecules* **1991**, *24*, 6263.
(18) Russell, T. P. *Mater. Sci. Rep.* **1990**, *5*, 171.
(19) Menelle, A.; Russell, T. P.; Anastasiadis, S. H.; Satija, S. K.; Majkrzak, C. F. *Phys. Rev. Lett.* **1992**, *68*.
(20) Foster, M. D.; Sikka, M.; Singh, N.; Bates, F. S.; Satija, S. K.; Majkrzak, C. F. *J. Chem. Phys.* **1992**, *96*, 8605.

(21) Russell, T. P.; Mayes, A. M.; Kunz, M. S. *Die Makromol. Chem.*, submitted.
(22) Olvera de al Cruz, M. *J. Chem. Phys.* **1989**, *90*, 1995.
(23) Savage, D. E.; Kleiner, J.; Schimke, N.; Phang, Y.-H.; Jankowski, T.; Jacobs, J.; Kariotis, R.; Lagally, M. G. *J. Appl. Phys.* **1991**, *69*, 1411.
(24) Kortright, J. B. *J. Appl. Phys.* **1991**, *70*, 3620.
(25) Sinha, S. K.; Sirota, E. B.; Garoff, S.; Stanley, H. B. *Phys. Rev. B.* **1988**, *38*, 2297.
(26) Sinha, S. K. *Physica B* **1991**, *173*, 25.
(27) Satija, S. K.; Sirota, E. B.; Hughes, G.; Sinha, S. K.; Russell, T. P. *J. Appl. Phys.*, submitted.
(28) Cai, Z. H.; Huang, K. G.; Montano, P. A.; Russell, T. P.; Bai, J. M.; Zajac, G. W. *J. Chem. Phys.* **1993**, *98*, 2376.
(29) Thomas, E. L.; Anderson, D. M.; Henkee, C. S.; Hoffman, D. *Nature* **1988**, *334*, 598.
(30) Hasagawa, H.; Tanaka, H.; Yamasaki, K.; Hashimoto, T. *Macromolecules* **1987**, *20*, 1651.
(31) Hashimoto, T.; Koizumi, S.; Hasegawa, H.; Izumitani, T.; Hyde, S. T. *Macromolecules* **1992**, *25*, 1433.
(32) Helfand, E. *Macromolecules* **1992**, *25*, 492.
(33) Mayes, A. M.; Russell, T. P.; Smith, G. S. Unpublished.
(34) Doi, M.; Edwards, S. F. *The Theory of Polymer Dynamicsm*; Clarendon Press: Oxford, 1986.
(35) Mayes, A. M.; Johnson, R. D.; Russell, T. P.; Smith, S. D.; Satija, S. K.; Majkrzak, C. F. *Macromolecules* **1993**, *26*, 1047.